Journal of The Electrochemical Society, **147** (1) 1-8 (2000)
S0013-4651(99)05-009-0 CCC: $7.00 © The Electrochemical Society, Inc.

A ^{119}Sn Mössbauer Spectrometry Study of Li-SnO Anode Materials for Li-Ion Cells

A. Hightower,*,[a] P. Delcroix,[b] G. Le Caër,[b] C-K. Huang,,[c] B. V. Ratnakumar,**,[c] C. C. Ahn,[a] and B. Fultz**,[a,z]**

[a] *Division of Engineering and Applied Science, California Institute of Technology, Pasadena, California 91125, USA*
[b] *Laboratoire de Science et Génie des Matériaux Métalliques, C.N.R.S. U.M.R. 7584, Ecole des Mines, F-54042 Nancy Cedex, France*
[c] *Jet Propulsion Laboratory, Electrochemical Technologies Group, Pasadena, California 91109, USA*

Anodes of SnO were charged reversibly with Li to capacities greater than 600 mAh/g. The anode materials were characterized by ^{119}Sn Mössbauer spectrometry at 11 and 300 K, and by X-ray diffractometry at 300 K. Trends in the valence of Sn were as expected when the Sn oxides are reduced in the presence of Li. At low Li capacities the SnO is reduced to small particles of β-Sn, and with increasing Li capacity an alloy of $Li_{22}Sn_5$ is formed. Although the $Li_{22}Sn_5$ develops over a range of Li concentrations in the anode material, the $Li_{22}Sn_5$ that forms at low Li insertions is not typical of bulk $Li_{22}Sn_5$ in either its structural or electrochemical properties. The recoil-free fraction of the Sn oxide (and perhaps the metallic Sn) in the anode materials showed an anomalously large temperature dependence. This is indicative of nanoparticles or a severely defective structure. We monitored the changes in the Li-SnO and Li-Sn materials during atmospheric exposure over times up to 2 months. This oxidation process of Sn was very much the reverse of the Sn reduction during the Li insertion, although it occurred over a much longer time scale. We also report the temperature dependencies of recoil-free fractions for standard samples of β-Sn, SnO_2, and the alloy $Li_{22}Sn_5$.

Manuscript submitted May 3, 1999; revised manuscript received August 3, 1999.

A high specific energy has generated widespread scientific and technical interest in Li-ion cells for secondary batteries. This high specific energy density is derived from the high cell voltage, typically 4 V (*vs.* 1.3 V for a typical Ni-MH secondary battery). The Li densities in the cathode and anode materials are modest, however, and it is hoped that higher capacities of these electrodes will lead to further increases in the specific energies of Li-ion cells. Anode and cathode materials are now subjects of numerous investigations.[1-3] Huggins performed some early work on alloy anodes.[4,5] Recently, Ioda *et al.*, of Fujifilm Celltec Co., Ltd., announced a new class of anode material comprising a composite Sn oxide glass.[6,7] These Sn oxide glasses have a reversible capacity of approximately twice that of carbon materials but unfortunately exhibit a large irreversible capacity and problems with capacity fade after tens of charge-discharge cycles.

Early evidence was that the Li inserted in the Sn oxide glass material was ionic,[7] but Courtney *et al.* have provided convincing evidence for the formation of metallic Sn and Sn-Li alloys during Li insertion.[8-10] The general picture is that Li will reduce the Sn oxides to metallic Sn. Further studies on the mechanism of Li insertion in tin oxides and alloys have been performed by Mao *et al.*[11,12] with ^{119}Sn Mössbauer spectrometry measurements using a sealed cell. With increasing Li concentration in the anode material, a series of Li-Sn phases were observed by X-ray diffractometry,[13] including $Li_{22}Sn_5$, which represents an increase in volume over that of pure β-Sn by a factor of 3.6. Courtney and Dahn argued that since the increase in specific volume induces large local stresses, the cycle life of the electrode is poor when the Sn-rich regions in the electrode are large.[8-13] The role of microstructure on cycle life of Sn oxide anodes remains poorly understood, however.

Althought the Fujifilm Celltec material has not yet been used for products in the marketplace, its promise has prompted a number of investigations into other Sn and Sn oxide materials that can be used as anodes in Li-ion cells.[9-18] One of the present authors has studied the insertion of Li into SnO,[14] showing again that the Li served to reduce the Sn, and a Li-Sn alloy was formed at higher Li concentrations. Here we report results of ^{119}Sn Mössbauer spectrometry measurements at 11 and 300 K on partially and fully charged Li-SnO anode materials. We present detailed measurements of the recoil-free fractions (RFF) of the anode materials, and we show that the RFFs of the Sn oxide in the anode is anomalous, indicative of atomic-scale heterogeneities in the distribution of Sn atoms. Similar results are reported for the β-Sn in the anode material, although the contribution from the β-Sn is not definitively resolved from the $Li_{22}Sn_5$. We also present results from a study on the deterioration of Li-charged anode materials and Li-Sn alloys during long-term atmospheric exposure. During atmospheric exposure, the selective oxidation of Li causes β-Sn to separate quickly from the Li-Sn alloy, and the β-Sn then oxidizes over longer times. The hyperfine parameters of the Mössbauer spectra indicate that in the early stages of oxidation, the Sn is in small or defective oxides with Sn^{4+}, but a little Sn^{2+} was observed at later times.

Experimental

Electrode and sample preparation.—Commercial SnO powder was purchased from Cerac Chemical. The SnO electrodes were fabricated on copper foil substrates using 6 wt % polyvinylidene fluoride (PVDF) binder with 10% carbon black as a conductive diluent. These electrodes were used in half-cells with Li metal as the anode and an electrolyte of 1 M $LiPF_6$ dissolved in 30% ethylene carbonate (EC) and 70% dimethylene carbonate DMC. Selected amounts of Li, varying from 0 to 6.4 mol per mol SnO, were titrated into SnO or extracted from Li_xSnO using galvanostatic measurements at a current density of 0.020 mA cm^{-2}. Here we define "*x*" in Li_xSnO as the molar ratio of Li to the initial SnO. Figure 1 shows the initial charge and discharge curves with labels indicating the approximate state of the samples used for Mössbauer spectrometry measurements. These samples are designated $Li_{2.3}SnO$ and Li_5SnO. Similar electrodes and cells were used in measurements of cycle life using an automatic battery cycler made by Arbin Corp., College Station, TX. Cycle life measurements were performed on sealed full cells with $LiCoO_2$ cathodes. The voltage range was controlled to be between 3.0 and 4.1 V with a charging current density of 0.2 mA/cm^2 and a discharging current density of 0.4 mA/cm^2. Cycle life measurements were also performed on a half-cell using a Li counter electrode. The cycle life measurements with half-cells used the same current densities for charging and discharging but a voltage range between 0 and 1 V.

To characterize the Li-SnO electrode materials by X-ray diffractometry (XRD), transmission electron microscopy (TEM), and Mössbauer spectrometry, after five cycles the electrodes were removed

* Electrochemical Society Student Member.
** Electrochemical Society Active Member.
z E-mail: btf@hyperfine.caltech.edu

S0013-4651(99)05-009-0 CCC: $7.00

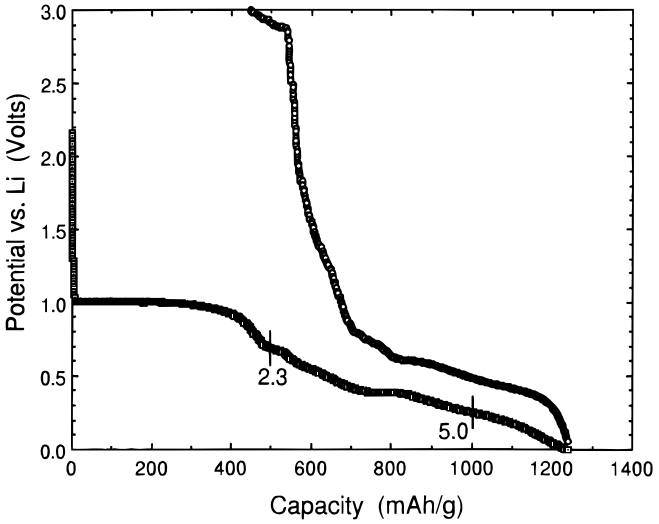

Figure 1. First pair of electrochemical charge and discharge curves on SnO anode at 0.02 mA/cm^2. Anodes for further analysis were obtained from samples charged initially to $x = 2.3$ and $x = 5$, as marked approximately on the figure.

from the half-cell and washed in DMC. The electrodes were vacuum dried and the powders were scraped. All operations were performed in a glove box with a pure and dry argon atmosphere. Samples for XRD were sealed in Pyrex capillary tubes under Ar atmosphere. TEM samples were prepared by crushing anode material with a mortar and pestle under Fluorinert FC-43 by 3M. Copper-backed, amorphous carbon grids were then dipped into the anode/Fluorinert suspension and inserted into the microscope. For Mössbauer spectrometry, the anode powder was mixed with a small amount of dehydrated boron nitride powders to ensure an overall thickness homogeneity. The samples were pressed into pellets that were encapsulated in altuglass sample holders and sealed with an altuglass glue. The samples comprised typically 50 mg of anode material. To study oxidation behavior, powdered samples were also stored in ambient laboratory air.

Mössbauer spectrometry.—^{119}Sn Mössbauer spectra were obtained at room temperature (denoted "RT," nominally 300 K) and at 11 K in transmission geometry with a spectrometer operated in the conventional constant acceleration mode. A $Ba^{119}SnO_3$ radiation source with a strength of ~10 mCi was used. Typical acquisition times were 12 or 24 h. All ^{119}Sn isomer shifts are referenced to $BaSnO_3$ at RT. The velocity scale was calibrated with a metallic body-centered cubic (bcc) iron sample and source of ^{57}Co in Rh. Spectra of commercially available powders of SnO_2, $BaSnO_3$, and a 12 μm foil of metallic β-Sn were also measured for use as calibration standards. Spectra of mixtures of known amounts of commercial powders of SnO_2, $Li_{22}Sn_5$, and β-Sn were also measured at 300 and 11 K.

All spectra were recorded with adequate counting statistics to permit a deconvolution of the natural linewidth from the spectrum. This deconvolution was useful for revealing the presence of different chemical environments of Sn atoms. The deconvolution utilized a conventional constrained Hesse-Rübatsch method.[19] The use of a model-independent histogram method for such an experimental purpose is new to the best of our knowledge. Since a simple Lorentzian lineshape is deconvoluted from the experimental spectra, in practice the deconvolution procedure is much the same as using the constrained Hesse-Rübatsch method for determining an isomer shift distribution. The calculation of hyperfine parameter distributions from spectra has been the subject of a number of studies and recent reviews.[19-22] Mathematically, this class of "inverse problems" is ill-posed. Small changes in spectra may lead to large changes in the resulting distributions. Regularization methods are therefore required when working with real experimental data, and regularization impairs the deconvolution procedure.[d]

Nevertheless, the deconvolution provides a significant and welcome improvement in resolution. For Sn spectra, the FWHM of the deconvoluted Lorentz line was chosen here as a typical minimum FWHM of a single Sn spectral line, that is, $\Gamma = 0.82$ mm/s. As another consequence of the regularization procedure, small oscillations appear above the flat zero background of the deconvoluted spectra. These oscillations are artifacts of the deconvolution procedure. Although the smoothing parameter must be small to avoid distorting excessively the main contributions, it must be large enough to avoid the oscillations that are driven by counting statistics.[e] All spectra were calculated with the same fitting conditions. The deconvoluted spectra are normalized to unity.

Electrochemical Results

Figure 1 shows the cell voltage *vs*. Li capacity for the first coulometric titration of the SnO electrode. The large irreversible capacity of about one-third the initial capacity (1240 mAh/g) was typical of cells of Sn oxide anode materials.[12-18] This irreversible capacity for the first cycle is probably caused by several factors, including the consumption of Li atoms during the reduction of the SnO, the reduction of the electrolyte with the formation of a solid-electrolyte interphase, and perhaps the formation of kinetically inaccessible Li. With $x > 6.2$, the cell voltage of 0 V indicates that there is an electroplating of Li on the electrode.

Cycle life results are presented in Fig. 2. The impressively high initial capacity declines markedly after several cycles, but the deterioration slows considerably after five cycles. After about 30 cycles the capacity was approximately 300 mAh/g in both the half-cell and full-cell cycling tests. These results are typical of results reported on other Sn oxide anodes.[10-18]

[d] Regularization conditions are set by the smoothing parameter of the constrained Hesse-Rübatsch method.[19] For example, when a Lorentzian line with a full-width-at-half-maximum (FWHM) $\Gamma_L = 0.22$ mm/s is removed from a calibration spectrum of metallic bcc iron (with a good signal-to-noise ratio) whose inner lines have a FWHM $\Gamma_M = 0.24$ mm/s, a line well approximated by a Gaussian line of FWHM $\Gamma_G = 0.13$ mm/s remains. This is much wider than the Lorentzian function of FWHM = 0.02 mm/s that is predicted.

[e] Such oscillations can have only a weak effect on the integral results presented in Tables I and II, however.

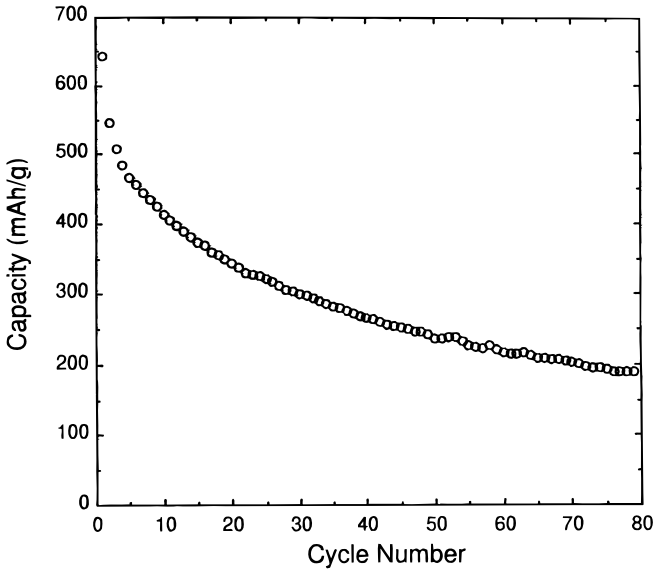

Figure 2. Capacity fade data on full cell of SnO anode with $LiCoO_2$ cathode with 0.43 mA/cm^2.

S0013-4651(99)05-009-0 CCC: $7.00

X-Ray Diffractometry and TEM Results

X-ray diffractometry was performed with Mo Kα radiation (λ = 0.07107 nm) using an Inel CPS120 powder diffractometer with a position-sensitive detector. The electrodes were composed initially of powdered SnO. Nevertheless, upon the first electrochemical titration of Li to $x = 5$ in Li_xSnO, XRD showed a distinct diffraction pattern from $Li_{22}Sn_5$ alone (see Fig. 3). The electrode material charged to $x = 2.3$ showed a mixture of β-Sn and $Li_{22}Sn_5$ but no SnO. Evidently the SnO is quickly reduced during Li insertion. When more Li is inserted, the β-Sn forms an alloy with Li metal. XRD shows this alloy to be $Li_{22}Sn_5$ both for low and high Li insertions, but the diffraction peaks from $Li_{22}Sn_5$ are broader for the electrode material charged to $x = 2.3$. Figure 3 also shows a significant broadening of the X-ray peaks from the β-Sn in the anode material, indicative of crystallite sizes of 10 nm or so. There was no evidence for oxides of either Sn or Li in any XRD patterns. From the large amounts of Sn^{4+} observed by Mössbauer spectrometry, we would expect a significant amount of diffraction from Sn oxides. The absence of diffraction peaks from Sn oxide indicates that it is probably amorphous, and its broad diffraction pattern was lost when stripping the diffraction pattern of the glass capillary from the measured data. Although we would expect only weak X-ray scattering from Li oxides, perhaps near the limit of detectability, we also suspect that the Li oxides may be amorphous or present as small particles with broadened diffraction peaks.

TEM was performed with a Philips EM430 transmission electron microscope operated at 200 keV. A bright-field transmission electron micrograph of the Li_5SnO material is presented in Fig. 4. The electron-beam damage to the specimen proved to be quick, substantial, and recognizable as a change in the shapes of the regions being examined. The image in Fig. 4 was acquired within a few seconds after the region was moved into the electron-beam. The diffraction pattern shows primarily β-Sn, although some diffraction spots from $Li_{22}Sn_5$ were visible in other diffraction patterns. On the other hand, this material was found to be primarily $Li_{22}Sn_5$ by XRD. The conversion to β-Sn suggests substantial oxidation of the thin TEM sample, as discussed below. The TEM image of Fig. 4 shows many small regions that appear dark, likely because they are β-Sn particles that are diffracting or more absorbing. These regions range in size from a few nanometers to tens of nanometers. The lighter regions are probably Li oxide.

Mössbauer Spectrometry Results

Mössbauer spectra of control samples.—At the top of Fig. 5 are transmission Mössbauer spectra from β-Sn, SnO_2, and $Li_{22}Sn_5$ acquired at 300 K (RT). Deconvoluted spectra with higher resolution

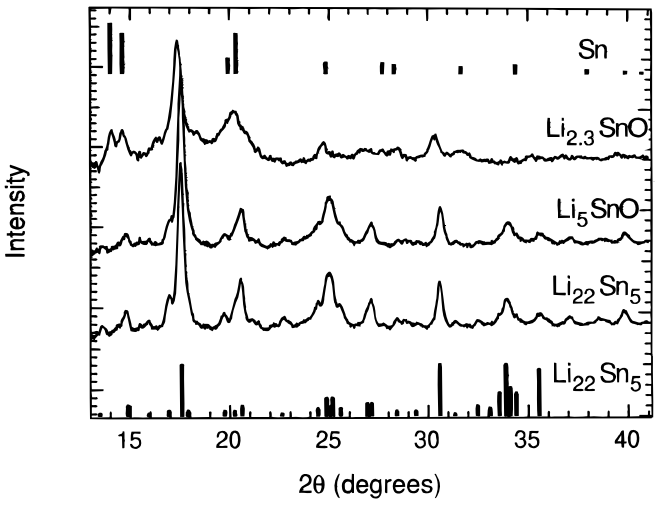

Figure 3. XRD patterns of $Li_{22}Sn_5$ alloy, and Sn oxide materials, Li_xSnO, charged initially to $x = 2.3$ and $x = 5$.

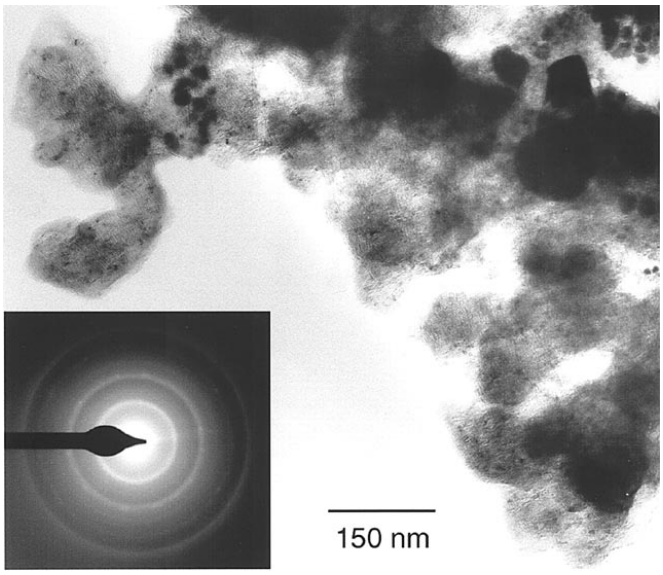

Figure 4. Bright-field TEM of the Li_5SnO material.

are shown below them. Also shown in Fig. 5 are deconvoluted spectra acquired at 11 K. In general, the more oxidized the Sn, the larger the shift to negative velocities. The SnO_2 spectrum at RT comprises a doublet of equal intensity lines with isomer shift = 0 ± 0.03 mm/s and a quadrupole splitting QS = 0.58 ± 0.04 mm/s. This is in good agreement with published values: QS = 0.50 mm/s,[23] QS = 0.61 mm/s,[24] QS = 0.55 or 0.56 mm/s,[25] QS = 0. 56 mm/s,[26] and QS = 0.54 mm/s [27]. The β-Sn spectrum at RT consists of a slightly broadened single line (Γ = 0.95 mm/s) with an isomer shift of 2.52 ± 0.03 mm/s at RT. It agrees with published values (IS = 2.56 ± 0.02 mm/s,[24] and 2.542 ± 0.005 mm/s [28]). It is important to note that the β-Sn isomer shift falls within the typical range (2.5-2.7 mm/s) of isomer shifts of Sn^{2+} in SnO or in SnO_x ($x < 2$) (the precise values depend on x and on the actual oxide structures). The β-Sn can be distinguished, however, because the oxide spectra exhibit quadrupole splittings larger than 1 mm/s and often close to 2 mm/s.[23-30] The isomer shift increases by about 0.04 mm/s when β-Sn is cooled to 77 K.[31] Theoretical calculations[32] show that the

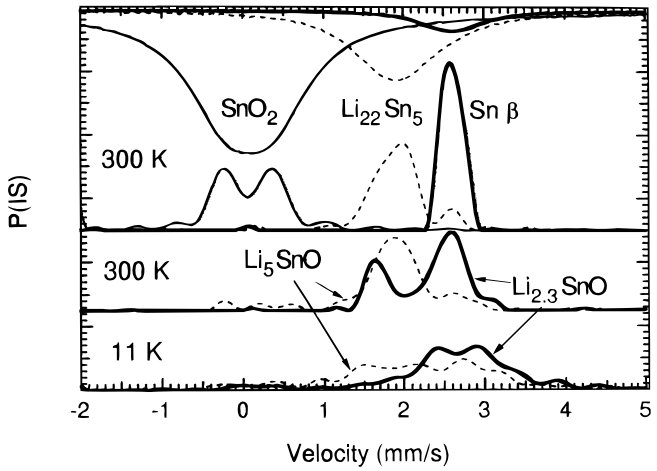

Figure 5. (Top) transmission Mössbauer spectra of β-Sn, $Li_{22}Sn_5$, and SnO_2 (RT). Below them are deconvoluted Mössbauer spectra of β-Sn, $Li_{22}Sn_5$, and SnO_2 (RT). (Middle) deconvoluted Mössbauer spectra from Sn oxide materials, Li_xSnO, charged to $x = 2.3$ and $x = 5$ (RT). (Bottom) deconvoluted Mössbauer spectra from Sn oxide materials, Li_xSnO, charged to $x = 2.3$ and $x = 5$ (11 K).

S0013-4651(99)05-009-0 CCC: $7.00

isomer shift of β-Sn falls between the isomer shift of covalent α-Sn, 2.021 ± 0.012 mm/s at RT,[28] and that of a hypothetical metallic face-centered cubic (fcc) Sn structure. A quadrupole splitting QS = 0.41 ± 0.04 mm/s is measured for β-Sn from the deconvoluted 11 K spectrum. Our data are in good agreement with results from recent theoretical calculations[33] of QS = 0.37 mm/s for β-Sn and QS = 0.47 mm/s for SnO_2.

Three spectra were measured from the control sample of $Li_{22}Sn_5$: one at RT, one at 11 K, and one again at RT after recording the low-temperature spectrum. The spectrum of $Li_{22}Sn_5$ is mainly a single broadened line. After deconvolution, a main line with a maximum at 1.93 ± 0.03 mm/s is observed. This line is asymmetric and a high-intensity shoulder at about 1.75 mm/s is also observed. A line with a relative area of 0.12 is also observed at 2.56 ± 0.03 mm/s. The deconvoluted RT spectrum in Fig. 5 also shows a much smaller broad line at about 1.05 mm/s which may not be experimentally significant, and very small oscillations that are artifacts of the deconvolution procedure. (These oscillations are considerably stronger for the 11 K deconvoluted spectrum owing to poorer counting statistics.) The crystallographic structure of $Li_{22}Sn_5$ is of the $Li_{22}Pb_5$ type (fcc, a = 1.978 nm, with 16 formula units). This structure contains 432 atoms per unit cell and 80 Sn atoms in four different Sn sites with respective proportions 0.2, 0.2, 0.3, 0.3. In principle, these four chemical environments contribute up to eight independent lines to the observed spectrum, but the resolution even of the deconvoluted spectra is inadequate to identify the eight independent peaks. We can say only that the broadening of the $Li_{22}Sn_5$ spectrum probably originates with the different crystallographic sites for Sn atoms in the $Li_{22}Sn_5$ structure. At 11 K, the spectrum is broadened significantly and rather symmetrically around 2.13 mm/s. This suggests an increase of the quadrupole splittings of the Sn sites when temperature is decreased. The isomer shift of approximately 2.0 mm/s for $Li_{22}Sn_5$ is consistent with α-Sn. We suggest, however, that the more negative isomer shift than that of β-Sn may have a chemical origin involving charge transfer between the Sn atoms and their Li neighbors.

The 300 K spectrum of $Li_{22}Sn_5$ measured subsequent to the 11 K spectrum is similar to the original 300 K spectrum but shows some differences. The main line is still at 1.95 ± 0.03 mm/s, but the shoulder at 1.75 mm/s is relatively more intense than previously. The relative area of the line at 2.56 mm/s has increased to 0.19, and a smaller line is seen at 1.25 mm/s. We show below that these changes are consistent with an oxidation of the sample.

From these results on the control samples, we present a convenient summary of the velocity ranges in ^{119}Sn spectra: −1.0 to 1.0 mm/s corresponds to Sn^{4+}; 1.0–2.3 mm/s corresponds to Sn in a Li-Sn alloy; and 2.2–3.2 mm/s corresponds to β-Sn. Spectral areas were integrated over these three velocity ranges to prepare Tables I and II for the different anode materials. For the spectra measured at 11 K, however, the overlap of the spectral components from β-Sn and the Li-Sn alloy required that their spectral components were fit to a pair of overlapping Gaussian lines. This fitting procedure was more ambiguous than integrating the areas of well-resolved lines, so we present error bars in Table I to indicate uncertainties in the area fractions. These areas, normalized by the recoil-free fractions, could be used to determine the fraction of Sn atoms in these three different chemical states.

Mössbauer spectra of anode materials.—Although the anode was prepared from SnO, Mössbauer spectrometry shows that the anode material of $Li_{2.3}SnO$ is a mixture of β-Sn plus a Li-Sn alloy, evidently $Li_{22}Sn_5$ from the XRD results. The fully lithiated anode material, Li_5SnO, is primarily $Li_{22}Sn_5$ from XRD, and its Mössbauer spectrum is quite close to that of the standard sample of $Li_{22}Sn_5$. It is not surprising that no SnO is present after five charge/discharge cycles, because we expect the Li to reduce SnO. Evidently the β-Sn forms with lower Li stoichiometry, perhaps less than $Li_{2.3}SnO$, and the $Li_{22}Sn_5$ forms at higher Li concentrations, accounting for all the Sn in the sample of Li_5SnO. This is approximately consistent with trends reported for other Sn oxide anode materials.[8-14] Owing to the low recoil-free fraction of β-Sn at RT, the fractions of spectral components in the spectrum acquired at 11 K are more representative of the actual phase fractions.

Table I. Relative spectral areas f_i (i = 1, 2, 3) at 300 K and at 11 K for the Sn^{4+}, Li-Sn alloy, and β-Sn contributions in Li_5SnO.

Sample	f_1 (Sn^{4+})	f_2 ($Li_{22}Sn_5$ alloy)	f_3 (β-Sn)
300 K as-prepared	0.09	0.80	0.11
At 11 K	0.13 ± 0.03	0.62 ∓ 0.12	0.25 ± 0.10
300 K after 11 K	0.10	0.59	0.31

[a] Errors represent uncertainties in the fitting procedure, which arise in the case of strongly overlapping subspectral components.

Table II. Relative spectral areas f_i (i = 1, 2, 3) at 300 K and at 11 K for the Sn^{4+}, Li-Sn alloy, and β-Sn contributions in $Li_{2.3}SnO$.

Sample	f_1 (Sn^{4+})	f_2 (alloy)	f_3 (β-Sn)
300 K as-prepared	0.01	0.36	0.63
At 11 K	0.07	0.10	0.83
300 K after 11 K	0.12	0.0	0.88

X-ray diffractometry (Fig. 3) shows that the $Li_{22}Sn_5$ intermetallic compound forms over a broad range of Li insertions, at least from $Li_{2.3}SnO$ to Li_5SnO. It seems that there are some differences in this compound for low and high Li insertions, however. The coulometric titration of Fig. 1 shows a change of voltage from 0.7 to 0.25 V between x = 2.3 and x = 5.0, although a short plateau is observed at 380 mV near x = 4 and can be associated with $Li_{22}Sn_5$.[34] The Mössbauer spectrum from the $Li_{22}Sn_5$ in the anode material of composition $Li_{2.3}SnO$ seems to be shifted toward more negative velocities than that of the material of composition of Li_5SnO (Fig. 5). Finally, the XRD peaks from the anode material of composition $Li_{2.3}SnO$ are broader than those from Li_5SnO (Fig. 3). We suggest that the $Li_{22}Sn_5$ that forms initially is more defective crystallographically than the $Li_{22}Sn_5$ that forms after more Li insertion. The chemical potential for Li in this more defective material is evidently lower than that of the more perfect $Li_{22}Sn_5$. Perhaps the crystallographic defects originate with a substoichiometry of Li, such as Li vacancies.

The change in the fractional contributions from the $Li_{22}Sn_5$ and the β-Sn after the sample of Li_5SnO was cooled to 11 K is probably insignificant, since there is strong overlap of these parts of the Mössbauer spectra. The sample of $Li_{2.3}SnO$ increased considerably its fraction of Sn^{4+} after cryogenic exposure, losing its alloy component and increasing the fraction of β-Sn. This is consistent with oxidation of the sample, since one of the windows on the sample package was not reliable upon cryogenic exposure. A detailed study of the oxidation behavior of these materials is presented below.

Recoil-free fractions: standards.—The recoil-free fraction (the efficiency of the Mössbauer effect for a ^{119}Sn nucleus in a given material at a specific temperature) is difficult to measure on an absolute basis. It is much easier to measure ratios of recoil-free fractions, which can be ratios of areas of spectral components of different phases, or ratios of areas of the same spectral component at different temperatures. For anode materials, we prefer the method of comparing the spectral areas of the same phase, since the phase fractions in a particular sample remain constant at different temperatures. Before using this method with anode materials, however, we first prepared four "standard" samples with known amounts of SnO_2 and β-Sn powders. Standard no. 1 had an approximately equal amount of Sn in the two phases (24 mg SnO_2 plus 20 mg β-Sn). Standard no. 2 had more β-Sn (8 mg SnO_2 plus 47 mg β-Sn), which ensured more

S0013-4651(99)05-009-0 CCC: $7.00

comparable spectral areas at higher temperatures. The other two standards were mixtures of known amounts of $Li_{22}Sn_5$ with either β-Sn or SnO_2. Standard no. 3 was 26.52 mg $Li_{22}Sn_5$ plus 13.42 mg SnO_2 and standard no. 4 was 15.44 mg $Li_{22}Sn_5$ plus 24.56 mg β-Sn.

The measured spectral intensities of the SnO_2, β-Sn, and $Li_{22}Sn_5$ at temperature, T, are the product of the recoil-free fractions, $f(T)$, and the atomic fractions, $x(T)$

$$I_{SnO_2}(T) = x_{SnO_2} f_{SnO_2}(T) \quad [1]$$

$$I_{\beta\text{-Sn}}(T) = x_{\beta\text{-Sn}} f_{\beta\text{-Sn}}(T) \quad [2]$$

$$I_{Li_{22}Sn_5}(T) = x_{Li_{22}Sn_5} f_{Li_{22}Sn_5}(T) \quad [3]$$

For comparison to literature results on β-Sn and SnO_2, we define the ratio, $R(T)$, as

$$R_{SnO_2/Sn}(T) \equiv \frac{f_{SnO_2}(T)}{f_{\beta-Sn}(T)} = \frac{x_{\beta-Sn} I_{SnO_2}(T)}{x_{SnO_2} I_{\beta-Sn}(T)} \quad [4]$$

We obtained $R_{SnO2/Sn}(11\text{ K}) = 1.74 \pm 0.30$ and $R_{SnO2/Sn}(11\text{ K}) = 1.40 \pm 0.30$ for Standard no. 1 and 2, respectively. With values in the literature of $f_{SnO_2}(11\text{ K}) = 0.89$ at 11 K,[35] and $f_{\beta\text{-Sn}}(10\text{ K}) = 0.715 \pm 0.01$,[36] we expect $R_{SnO2/Sn}(11\text{ K}) = 1.24$, in reasonable agreement with our results. At RT we find $R_{SnO2/Sn}(300\text{ K}) = 8.4 \pm 0.8$. At RT, the Lamb-Mössbauer factors are reported to be $f_{SnO_2}(300\text{ K}) = 0.56$,[27] $f_{SnO_2}(300\text{ K}) = 0.473$,[29] and $f_{\beta\text{-Sn}}(300\text{ K}) = 0.04 \pm 0.01$,[36] $f(300\text{ K}) = 0.060 \pm 0.002$,[37] although for 25 nm nanoparticles of Sn $f_{\beta\text{-Sn}}(300\text{ K}) = 0.022 \pm 0.001$.[37] These previously published values give a range of $R_{SnO2/Sn}(300\text{ K})$ from 8 to 14, again in reasonable agreement with the results on our standard samples.

The standard samples composed of $Li_{22}Sn_5$ plus β-Sn, and $Li_{22}Sn_5$ plus SnO_2, were measured at RT, at 11 K, and again at RT. It was found that the sample was unstable over periods of weeks, forming some β–Sn when the Li reacted with the O. Nevertheless, from the spectra measured promptly at RT, we found

$$R_{Sn/LiSn}(\text{RT}) \equiv \frac{f_{\beta Sn}(\text{RT})}{f_{Li_{22}Sn_5}(\text{RT})} = \frac{x_{Li_{22}Sn_5} I_{\beta Sn}(\text{RT})}{x_{\beta Sn} I_{Li_{22}Sn_5}(\text{RT})} = 0.50 \pm 0.10 \quad [5]$$

$$R_{LiSn/SnO_2}(\text{RT}) \equiv \frac{f_{Li_{22}Sn_5}(\text{RT})}{f_{SnO_2}(\text{RT})} = \frac{x_{SnO_2} I_{Li_{22}Sn_5}(\text{RT})}{x_{Li_{22}Sn_5} I_{SnO_2}(\text{RT})} = 0.60 \pm 0.10 \quad [6]$$

Evidently the $Li_{22}Sn_5$ alloy has a larger effective Debye temperature than β-Sn, although smaller than SnO_2. The sample of $Li_{22}Sn_5$ plus β-Sn, which was more stable against Li oxidation, showed as expected at 11 K that the RFFs of $Li_{22}Sn_5$ and β-Sn were similar

$$R_{Sn/LiSn}(11\text{ K}) \equiv \frac{f_{\beta Sn}(11\text{ K})}{f_{Li_{22}Sn_5}(11\text{ K})} = \frac{x_{Li_{22}Sn_5} I_{\beta Sn}(11\text{ K})}{x_{\beta Sn} I_{Li_{22}Sn_5}(11\text{ K})} = 1.0 \pm 0.2 \quad [7]$$

We attempted to obtain Debye temperatures from our standards, and found: 277 K for SnO_2, 212 K for $Li_{22}Sn_5$, and 134 K for β-Sn. Errors may be about ±20 K.

Recoil-free fractions: anode materials.—It might be expected that the phase fractions of the Li_5SnO anode material can be determined with the recoil-free fraction information from the standard samples. Qualitative phase fractions can be obtained from Tables I and II, but we cannot quantify them further owing to the following interesting phenomenon.

Mössbauer spectra from the sample of Li_5SnO were measured at 11 and 300 K. We can use Eq. 1 and 2 to eliminate the phase fractions to compare the temperature dependencies of the recoil-free fractions

$$\mathcal{R}_{SnO_2/Sn} \equiv \frac{R_{SnO_2/Sn}(\text{RT})}{R_{SnO_2/Sn}(11\text{ K})} = \frac{I_{SnO_2}(\text{RT}) I_{\beta Sn}(11\text{ K})}{I_{\beta Sn}(\text{RT}) I_{SnO_2}(11\text{ K})} \quad [8]$$

Using our own experimental results from the calibration standards, we obtain $\mathcal{R}_{SnO2/Sn} = 5.4$. From the data in Table I for the anode material of Li_5SnO, we obtain $\mathcal{R}_{SnO2/Sn} = 1.5 \pm 0.4$.

The unexpectedly different result for $\mathcal{R}_{SnO2/Sn}$ for the standards and for the anode material is well beyond expected errors and can have two explanations. When comparing the SnO_2 and the β-Sn, either the effective Debye temperature of the β-Sn in the anode materials is higher than that of the β-Sn in the control sample, or the Debye temperature of the Sn^{4+} in the anode material (nominally SnO_2) is lower than that of the Sn^{4+} in the control sample of SnO_2. We cannot prove one case or the other from the measurements we have performed. One argument is that the Debye temperature of the SnO_2 in the anode material is lower than that of the control sample, because atomic-scale defects in oxide structure can suppress the Debye temperature. Assuming the β-Sn in the anode material to have a Debye temperature of 134 K, we obtain a Debye temperature of 146 K for the the Sn^{4+} in the anode material. Another argument is that electropositive Li neighbors may increase the phonon frequencies of β-Sn. We expect that electropositive Li neighbors can alter one way or another the phonon frequencies of β-Sn,[38] but it is unclear if the frequencies will increase when the small β-Sn particles are of 10 nm spatial dimensions. We consider it less likely that the anomalous behavior of $\mathcal{R}_{SnO2/Sn}$ originates with a stiffening of the vibrational frequencies in the β-Sn, which would need a Debye temperature close to that of SnO_2. Either case, however, requires that the microstructure of the anode material contain disorder on nanometer or subnanometer dimensions.

In the same way, by comparing the RFFs of the $Li_{22}Sn_5$ alloy and β-Sn we find $\mathcal{R}_{Sn/Li22Sn5} = 0.2$ for calibration standards, and $\mathcal{R}_{Sn/Li22Sn5} = 0.35$ for the anode material of Li_5SnO. We consider this discrepancy insignificant, however, because of the difficulty of resolving the two overlapping contributions to the Mössbauer spectra at 11 K. We cannot reliably report an anomaly in the RFF ratio of the β-Sn and the $Li_{22}Sn_5$ in the anode material. It is known, however, that the Debye temperature of nanoparticle Sn is low,[37] so it is possible that the Debye temperature of the $Li_{22}Sn_5$ in the anode material is also suppressed.

One might expect to use the results from XRD to quantify the fractions of phases in the anode material, but we detected no SnO_2 in the XRD patterns. We offer the following interpretation of these results on the SnO_2 in the anode material. First, the Mössbauer spectrometry tells us only that the Sn is Sn^{4+}, not necessarily the structure of crystalline bulk SnO_2. The hyperfine parameters of the Sn^{4+} in the anode material differ from those reported in bulk SnO_2. In the next section we describe how the Sn^{4+} spectrum of the anode materials evolved to that characteristic of SnO_2 when the anode material was exposed to ambient air over a long period of time. The initial Sn^{4+} in the anode material is not in the expected local structure of SnO_2. The absence of distinct XRD peaks indicates that the Sn^{4+} oxide is either present as extremely small particles or as an amorphous phase (or both). The anomalous ratio of $\mathcal{R}_{SnO2/Sn}$ for Sn in the electrode material tends to support the interpretation of small particles, although an amorphous oxide could also have a low recoil-free fraction and would be less visible in an XRD pattern.

Oxidation in Ambient Air

Figures 6 and 7 present XRD patterns from the $Li_{2.3}SnO$ and Li_5SnO materials during long-term exposure to ambient air at 300 K. All samples show the same trends, and oxidation proceeds in two stages. The initial Li-Sn alloy undergoes a separation into β-Sn and Li oxide over a period of about 30 min for the $Li_{2.3}SnO$ and several hours for the Li_5SnO anode material. This process is followed by a much slower oxidation of the β-Sn by the formation of SnO_2 observed by Mössbauer spectrometry.

Figures 8-10 present Mössbauer spectra from the $Li_{2.3}SnO$, Li_5SnO, and $Li_{22}Sn_5$ materials, respectively, during long-term exposure to ambient atmosphere at 300 K. All samples show the same trends, and these trends are in good agreement with the results from XRD. The initial Li-Sn alloy[f] undergoes a separation into β-Sn and

[f] The small amount of Sn^{4+} in the starting material could be associated with oxide regions kinetically inaccessible to Li, or a surface oxidation associated with inadvertent atmospheric exposure.

S0013-4651(99)05-009-0 CCC: $7.00

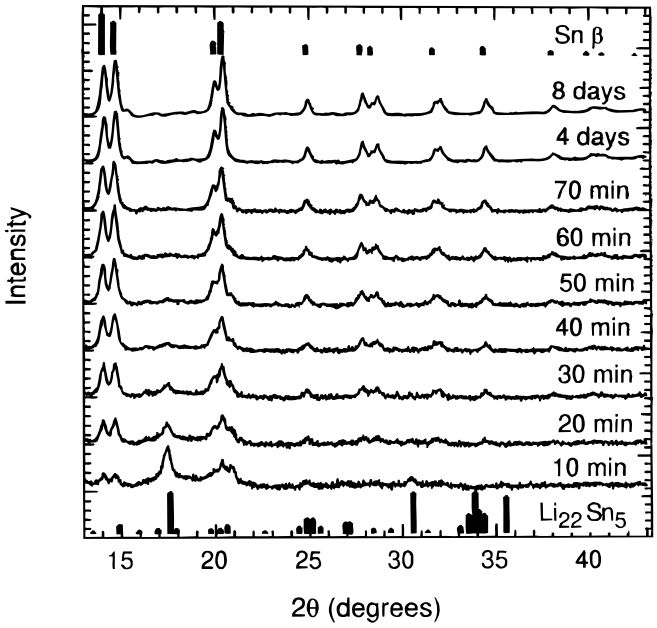

Figure 6. XRD patterns from $Li_{2.3}SnO$ anode material exposed to ambient air for various times.

Li oxide, without the formation of Sn^{4+}. This process is followed by a much slower oxidation of the β-Sn by the formation of Sn^{4+}, which approaches the spectrum of SnO_2. In the early stages of oxidation, for the three materials $Li_{2.3}SnO$, Li_5SnO, and $Li_{22}Sn_5$, the hyperfine parameters of the Sn^{4+} differ from those of crystalline SnO_2, but both samples show a trend toward a symmetric quadrupole doublet, approaching it over 100 days or so. Since the SnO_2 formation was observed clearly by Mössbauer spectrometry but not by XRD, we suggest that this oxide has an amorphous structure.

The spectra of $Li_{22}Sn_5$ exposed to air for more than 100 days show two small peaks at 1.89 mm/s and at 3.61 mm/s with QS = 1.72 ± 0.04 mm/s and IS = 2.75 ± 0.04 mm/s, which are typical of Sn^{2+} in SnO.[23-26,30,39] The hyperfine parameters depend on the structure, and the parameters found here agree with those of amorphous $Sn^{2+}O$ [39] and of ultrafine oxidized Sn particles,[25] but not with those of crystalline tetragonal SnO.[40,41]

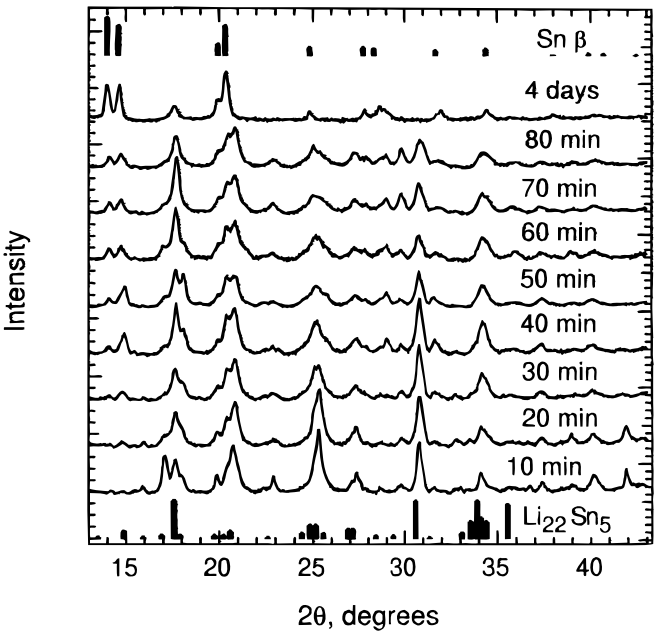

Figure 7. XRD patterns from Li_5SnO anode material exposed to ambient air for various times.

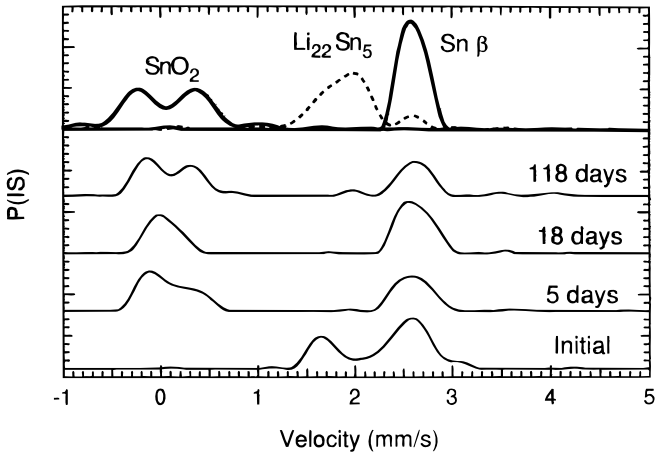

Figure 8. Deconvoluted RT Mössbauer spectra from $Li_{2.3}SnO$ anode material exposed to ambient air for various times.

We observed a curious small peak at 4 mm/s in the anode material undergoing oxidation. This peak is probably real, but is not easy to understand. It could be one peak of a quadrupole doublet from an environment with a large electric field gradient, for instance, surface SnO, Sn_2O_3, or amorphous SnO_x. Perhaps it originates with an unusual crystal structure of Sn such as electrochemically prepared allotropic forms of Sn "α2-Sn,"[42-45] such as fcc diamond type[42] with lattice parameters of about 5.66 A for IS about 4.10 mm/s. Reference 44 gives QS = 0, IS = 4.08 ± 0.05 mm/s.

Thermodynamics of Anode Reactions and Oxidation

The initial insertion reaction of Li into SnO is the energetically favorable reaction of Li oxidation, which occurs with a change in chemical potential of the Li atom of about 3 eV with respect to the Li metal reference electrode. The capacity of this reaction to consume Li is much smaller than the subsequent reaction at about 0.5 V, which involves the formation of a Li-rich Li-Sn alloy, evidently the compound $Li_{22}Sn_5$. Experimental evidence for these two reactions is seen in Fig. 1 at the voltages of 3 and 0.4 V. Note, however, that the first reaction of Li oxidation has a much larger capacity than expected from the formation of Li_2O or LiO. We attribute this excessive consumption of Li to the decomposition of electrolyte, for example, as in the formation of the surface-electrolyte interphase (SEI). Neither the oxidation of Li in reacting with SnO, nor the oxidation of Li

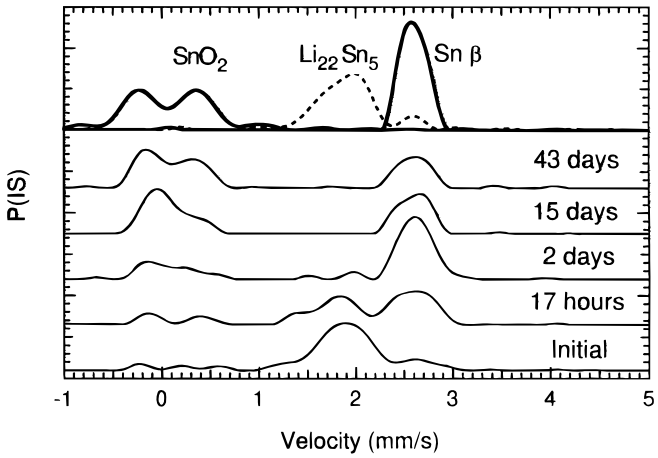

Figure 9. Deconvoluted RT Mössbauer spectra from Li_5SnO anode material exposed to ambient air for various times.

S0013-4651(99)05-009-0 CCC: $7.00

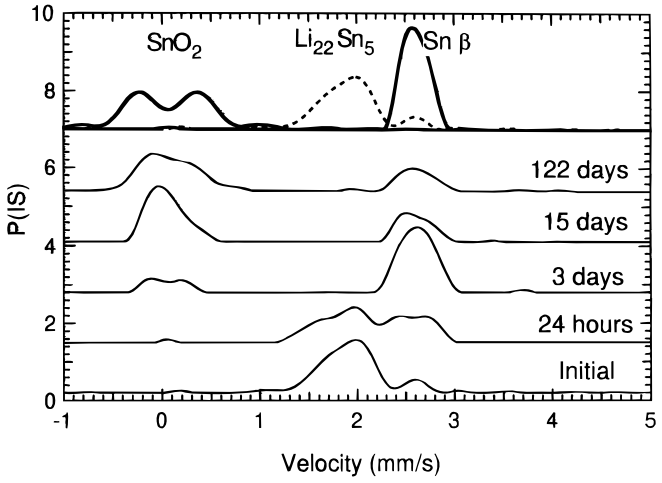

Figure 10. Deconvoluted RT Mössbauer spectra from $Li_{22}Sn_5$ alloy exposed to ambient air for various times.

during electrolyte decomposition, are reversible reactions in normal cell operation.

The second reaction below 0.8 V with respect to the Li reference electrode is reversible in normal cell operation. In some Sn oxide anode materials the formation of a Li-Sn alloy may occur in stages involving a number of intermediate alloy compounds,[8-14,41] but for our initial SnO anode we find evidence only for the formation of the $Li_{22}Sn_5$ intermetallic compound. From the data of Fig. 1, it appears that when the Sn is fully used in this compound, the subsequent reaction is the deposition of Li metal on the anode. This is the third reaction shown at 0.0 V. This reaction is perhaps electrochemically reversible, but it is likely that the electroplating of Li causes changes to the anode or SEI.

With the exposure of the anode material to oxygen in the ambient air, the system is opened and new reactions occur. The first reaction is the same as occurs in the first charging of an electrochemical cell, that is, more Li will oxidize. This reaction is favored thermodynamically more than the oxidation of the Sn, but oxidation of the Sn is expected once the Li is consumed. The data of Fig. 6-10 show that the oxidation of the Li occurs in tens of minutes, whereas the Sn oxidation occurs over tens of days. The oxidation of Li is strongly favored kinetically over the oxidation of Sn, suggesting that a higher diffusive mobility of Li atoms than Sn atoms may play a role in the kinetics of oxidation.

The total free energy change of each reaction must be favorable. In the first reaction of lithiation of SnO or oxidation of the anode material in air, for example, the Li oxides must be more stable than the Sn oxides if Li oxidation is to occur. This is true, with the difference in standard energies of formation of these compounds being about 30 kJ/mol. The chemical bonds involving Li are stronger than those involving Sn, and the electrode reactions can be understood by consideration of the Li alone. The exception is the final oxidation of Sn in ambient air, which does not involve further changes to any Li. It is interesting that per Sn atom, the standard free energies of formation of SnO and SnO_2 are not very different, being -252 and -258 kJ/mol, respectively. Mössbauer spectrometry showed that the formation of Sn^{4+} in a structure related to SnO_2 was the dominant reaction during the exposure of $Li_{22}Sn_5$ to ambient air. With increasing time, however, we found evidence for the formation of a small amount of Sn^{2+} (as in SnO) by the appearance of a weak Mössbauer peak at about 4 mm/s.

Conclusions

Mössbauer spectrometry and XRD measurements were performed on anode materials of SnO in which Li was inserted electrochemically. These measurements were interpreted with the aid of results on standard samples prepared from β-Sn, $Li_{22}Sn_5$, and SnO_2, measured at room temperature and 11 K. In anode materials, at low Li capacities the SnO is reduced to small particles of β-Sn. The Sn^{4+} in the anode material had an anomalous temperature dependence of its recoil-free fraction, indicating a severely defective structure on the atomic scale. The lack of XRD peaks from a Sn oxide indicates that the Sn^{4+} is in an amorphous oxide and may have small spatial features as well. With increasing Li concentration, there was first the formation of β-Sn as small particles of ~10 nm dimension, and Li oxide, which may have been amorphous. With more Li insertion, a Li-Sn alloy was formed. This alloy seems to have been exclusively the $Li_{22}Sn_5$ intermetallic compound. Although the $Li_{22}Sn_5$ develops over a range of Li concentrations in the anode material, from XRD it appears that at low Li insertions the $Li_{22}Sn_5$ is more defective than bulk $Li_{22}Sn_5$. From coulometric titrations, this crystallographically defective $Li_{22}Sn_5$ appears to have a more favorable chemical potential for Li atoms.

Although the reactions in SnO-Li electrode materials involve all atom species, the thermodynamic tendencies for these reactions were dominated by the chemical preferences of the Li atoms. The voltages of these reactions show that the initial insertion of Li into SnO is accompanied by an additional oxidation of Li, which we interpret as electrolyte decomposition in the formation of an SEI, for example. The irreversible capacity for this initial insertion of Li is large, being 500 mAh/g. The remaining cycles are largely reversible, with Li atoms inserting into and deinserting from metallic alloys that include $Li_{22}Sn_5$. While the early cycles showed an excellent reversible capacity of greater than 600 mAh/g, the material has an unfortunately short cycle life of perhaps 30 cycles.

We also studied the oxidation of Li-charged anode materials and Li-Sn alloys during long-term atmospheric exposure. The oxidation tendencies involved a quick selective oxidation of Li that occurred over tens of minutes. Metallic β-Sn was observed during this separation of the Li-Sn alloy. The β-Sn then oxidized over longer times of weeks, forming primarily Sn^{4+} but later a small amount of Sn^{2+}. The hyperfine parameters of the Mössbauer spectra indicate that in the early stages of oxidation of the Sn, there is a formation of amorphous, small, or highly defective oxides with Sn^{4+}.

Acknowledgments

We thank Professor B. Malaman (Universite Henri Poincare, Nancy I) for useful discussions. The work at Caltech was supported by DOE through Basic Energy Sciences grant no. DE-FG03-94ER14493.

California Institute of Technology assisted in meeting the publication costs of this article.

References

1. *Lithium Batteries, New Materials, Development and Perspectives*, G. Pistoia, Editor, Elsevier, New York (1994).
2. *Lithium Batteries*, J.-P. Gabano, Editor, Academic Press, New York (1983).
3. *Materials Research Society Symposium Proceedings 393*, D. H. Doughty, B. Vyas, T. Takamura, and J. R. Huff, Editors, MRS, Pittsburgh, PA (1995).
4. B. A. Boukamp, G. C. Lesh, and R. A. Huggins, *J. Electrochem. Soc.*, **128**, 725 (1981).
5. R. A. Huggins and B. A. Boukamp, U.S. Pat. 4,436,796 (1984).
6. Y. Idota, M. Mishima, Y. Miyaki, T. Kubota, and T. Miyasaka, Eur. Pat. 651,450A1 (1995); Y. Idota, U.S. Pat. 5,478,671 (1995).
7. Y. Idota, T. Kubota, A. Matsufuji, Y. Maekawa, and T. Miyasaka, *Science*, **276**, 1395 (1997).
8. I. A. Courtney and J. R. Dahn, *J. Electrochem. Soc.*, **144**, 2943 (1997).
9. I. A. Courtney and J. R. Dahn, *J. Electrochem. Soc.*, **144**, 2045 (1997).
10. I. A. Courtney, W. R. McKinnon, and J. R. Dahn, *J. Electrochem. Soc.*, **146**, 59 (1999).
11. O. Mao, R. A. Dunlap, I. A. Courtney, and J. R. Dahn, *J. Electrochem. Soc.*, **145**, 4195 (1998).
12. O. Mao, R. A. Dunlap, and J. R. Dahn, *J. Electrochem. Soc.*, **146**, 405 (1999).
13. O. Mao and J. H. Dahn, *J. Electrochem. Soc.*, **146**, 414 (1999).
14. Y. Wang, J. Sakamoto, C. K. Huang, S. Surampudi, and S. G. Greenbaum, *Solid State Ionics*, **110**, 167 (1998).
15. T. Brousse, R. Retoux, U. Herterich, and D. M. Schleich, *J. Electrochem. Soc.*, **145**, 1 (1998).
16. W. Liu, X. Huang, Z. Wang, H. Li, and L. Chen, *J. Electrochem. Soc.*, **145**, 59 (1998).
17. S. C. Nam, Y. H. Kim, W. I. Cho, B. W. Cho, H. S. Chun, and K. S. Yun, *Electrochem. Solid-State Lett.*, **2**, 9 (1999).
18. R. A. Dunlap, O. Mao, and J. R. Dahn, *Phys. Rev. B*, **59**, 3494 (1999).

S0013-4651(99)05-009-0 CCC: $7.00

19. G. Le Caër and J. M. Dubois, *J. Phys. E: Sci. Instrum.*, **12**, 1083 (1979).
20. G. Le Caër and R. A. Brand, *J. Phys.: Cond. Matter*, **10**, 10715 (1998).
21. S. J. Campbell and F. Aubertin, in *Mössbauer Spectroscopy Applied to Inorganic Chemistry*, Vol. 3, G. Long, Editor, Plenum Press, New York (1988).
22. D. Rancourt, in *Mössbauer Spectroscopy Applied to Magnetism and Materials Science*, Vol. 2, G. Long and F. Grandjean, Editors, p. 105, Plenum, New York (1996).
23. B. Stjerna, C. G. Granqvist, A. Seidel, and L. Häggström, *J. Appl. Phys.*, **68**, 6241 (1990).
24. M. S. Moreno, R. C. Mercader, and A. G. Bibiloni, *J. Phys.: Cond. Matter*, **4**, 351 (1992).
25. C. H. Shek, J. K. L. Lai, G. M. Lin, Y. F. Zheng, and W. H. Liu, *J. Phys. Chem. Solids*, **58**, 13 (1997).
26. J. Isidorsson, C. G. Granqvist, L. Häggström, and E. Nordström, *J. Appl. Phys.*, **80**, 2367 (1996).
27. J. L. Solis, J. Frantti, V. Lantto, L. Häggström, and M. Wikner, *Phys. Rev. B*, **57**, 13491 (1998).
28. J. G. Stevens and W. L. Gettis, *Isomer Shift Reference Scales*, Mössbauer Effect Data Center, University of North Carolina, Asheville, NC (1981).
29. M. S. Moreno and R. C. Mercader, *Phys. Rev. B*, **50**, 9875 (1994).
30. H. G. Neumann, P. Zeggel, and K. Melzer, *J. Non-Cryst. Sol.*, **108**, 128 (1989).
31. G. M. Rothberg, S. Guimard, and N. Benczer-Koller, *Phys. Rev. B*, **1**, 136 (1970).
32. A. Svane, *Phys. Rev. Lett.*, **60**, 2693 (1988).
33. A. Svane, N. E. Christensen, C. O. Rodriguez, and M. Methfessel, *Phys. Rev. B*, **55**, 12572 (1997).
34. J. Q. Wang, I. D. Raistrick, and R. A. Huggins, *J. Electrochem. Soc.*, **133**, 457 (1986).
35. M. S. Moreno and R. C. Mercader, *Hyperfine Interact.*, **83**, 415 (1994).
36. C. Hohenemser, *Phys. Rev.*, **139**, A185 (1965).
37. I. P. Suzdalev, M. Ya Gen, V. I. Gol'danskii, and E. F. Makarov, *Sov. Phys. JETP*, **24**, 79 (1967).
38. V. Ozolins and A. Zunger, *Phys. Rev. Lett.*, **82**, 767 (1999).
39. G. S. Collins, T. Kachnowski, N. Benczer-Koller, and M. Pasternak, *Phys. Rev. B*, **19**, 1369 (1979).
40. M. Renteria, A. G. Bibiloni, M. S. Moreno, J. Desimoni, R. C. Mercader, A. Bartos, M. Uhrmacher, and K. P. Lieb, *J. Phys. Cond. Matter*, **3**, 3625 (1991).
41. J. Sangster and C. W. Bale, *J. Phase Equilib.*, **19**, 70 (1998).
42. V. Rusanov, T. S. Bonchev, I. Mandjukov, and M. Mihov, *J. Phys. F: Metal Phys.*, **16**, 515 (1986).
43. V. Rusanov, I. Mandjukov, T. S. Bonchev, and K. Kantchev, *J. Phys. F: Metal Phys.*, **18**, 1311 (1988).
44. S. K. Peneva, N. S. Neykov, and K. D. Djuneva, *Z. Kristall.*, **202**, 191 (1992).
45. S. K. Peneva, N. S. Neykov, V. Rusanov, and D. D. Chakarov, *J. Phys.: Condens. Matter*, **6**, 2083 (1994).